Improvement of Medium-Range Forecasts Using the Analog-Dynamical Method

HAIPENG YU, JIANPING HUANG, AND JIFAN CHOU

College of Atmospheric Sciences and Key Laboratory for Semi-Arid Climate Change of the Ministry of Education, Lanzhou University, Lanzhou, China

(Manuscript received 9 August 2013, in final form 20 November 2013)

ABSTRACT

This study further develops the analog-dynamical method and applies it to medium-range weather forecasts. By regarding the forecast field as a small disturbance superimposed on historical analog fields, historical analog errors can be used to estimate and correct forecast errors. This method is applied to 10-day forecasts from the Global and Regional Assimilation and Prediction System (GRAPES). Both the distribution of atmospheric circulation and the pattern of sea surface temperature (SST) are considered in choosing the analog samples from a historical dataset for 2001–10 based on NCEP Final (FNL) data. The results demonstrate that the analog-dynamical method greatly reduces forecast errors and extends the period of validity of the global 500-hPa height field by 0.8 days, which is superior to results obtained using systematic correction. The correction effect at 500 hPa is increasingly significant when the lead time increases. Although the analogs are selected using 500-hPa height fields, the forecast skill at all vertical levels is improved. The average increase of the anomaly correlation coefficient (ACC) is 0.07, and the root-mean-square error (RMSE) is decreased by 10 gpm on average at a lead time of 10 days. The magnitude of errors for most forecast fields, such as height, temperature, and kinetic energy is decreased considerably by inverse correction. The model improvement is primarily a result of improvement for planetary-scale waves, while the correction for synoptic-scale waves does not affect model forecast skill. As this method is easy to operate and transport to other sophisticated models, it could be appropriate for operational use.

1. Introduction

The capabilities of numerical weather forecasting have developed significantly as a result of the increasing accumulation of observational data, advanced data assimilation, and more sophisticated models. However, forecast errors are still considerable and further improvements are required. Errors can be attributed to two factors: inaccurate initial conditions and model deficiencies. The errors in initial conditions have been substantially reduced as a result of the development of data assimilation and ensemble forecasting, making model deficiencies a far more important factor (Kalnay 2002). Generally, model errors can be reduced by increasing model resolution and improving physical parameterizations, but they cannot be eliminated as the model develops. As a result, it is necessary to develop empirical strategies to account for model errors as a supplement to the general strategy.

The strategies and methodologies to correct model errors can be classified into state-dependent corrections and state-independent corrections (Danforth and Kalnay 2008a). The latter are independent of models and are frequently used, such as model output statistics (Glahn and Lowry 1972) and nudging (Johansson and Saha 1989; Kaas et al. 1999; Klinker and Sardeshmukh 1992; Saha 1992; Yang et al. 2008; Yang and Anderson 2000).

Mean-square forecast error can be divided into systematic and nonsystematic components, with systematic components contributing about 20% (Dalcher and Kalnay 1987). Model deficiencies can lead to both systematic and nonsystematic errors (Reynolds et al. 1994), while some results have indicated that state-independent correction can only reduce systematic components (DelSole and Hou 1999; DelSole et al. 2008; Saha 1992). This suggests that state-dependent correction is needed to reduce nonsystematic errors. One effective method is to establish a statistical relationship between the tendency

Denotes Open Access content.

Corresponding author address: Jianping Huang, College of Atmospheric Sciences, Lanzhou University, No. 222 Tianshui South Rd., Lanzhou, 730000, China.
E-mail: hjp@lzu.edu.cn

DOI: 10.1175/MWR-D-13-00250.1

errors and model state (Leith 1978). DelSole and Hou (1999) developed such a method for a nonlinear quasigeostrophic model and found that forecast skill was improved. However, computations of the cross variance have been found to be prohibitive for operational use (Danforth et al. 2007). Using the singular-value decomposition of coupled analysis correction and forecast state anomalies, Danforth and Kalnay (2008b; Danforth et al. 2007) greatly reduced the computational expense, but the global average improvement was minimal because the correction was made locally in space and time. The commonality of these methods is the requirement of a sample time series to estimate the error covariance; therefore, the statistical relationship depends on the samples selected and it is difficult to maintain consistent results.

For linear systems, it is effective to establish statistical relationships to correct model errors, and using more historical data yields better results. However, this is not the case for nonlinear systems, which require more data pertinence rather than simply a large quantity of data. Alternatively, analog states in historical observation datasets may have similar characteristics to the current state, and can be taken into account to estimate and correct state-dependent errors. As a phenomenon of atmospheric nonlinear evolution, analogs have been widely used in forecast and predictability studies. Lorenz (1969) used naturally occurring analogs to ensure the error growth would reflect predictability. His results also indicated that the likelihood of encountering true analogs is small, as confirmed by Van den Dool (1994). Barnett and Preisendorfer (1978) avoided this problem by using the analog climate state vector in the multidimensional EOF space of multiple datasets. In short, analog forecasting has been much developed and used operationally in the National Centers for Environmental Prediction (NCEP; Livezey and Barnston 1988).

With regard to the traditional analog forecast, it is an oversimplification to regard the current state as a repeat of the historical states. Combining analog states with a dynamical model is expected to be beneficial, so the so-called analog-dynamical approach has been developed. When the forecast state is regarded as a small disturbance superimposed on a historical analog field, statistical techniques can be used in combination with a dynamical forecast (Chou 1979). By estimating the current tendency error with that of an analog state, a deviation equation is obtained in the quasigeostrophic model and an improved forecast performance is achieved (Qiu and Chou 1989). On this basis, Huang et al. (1993) established a coupled analog deviation model for monthly and seasonal forecasts and achieved better results compared with the statistical analog method. This method has been applied to forecasts of the monthly mean circulation in an operational T63L16 model, with results superior to the control forecasts (Bao et al. 2004). A similar methodology was proposed independently by D'Andrea and Vautard (2000), who used a method similar to four-dimensional variational assimilation to estimate the initial tendency errors of analog samples. However, the complexity involved in establishing an adjoint model has limited its operational applications. Ren and Chou (2007) and Ren et al. (2006) estimated forecast error instead of tendency error using analog techniques to avoid establishing an analog deviation model. They obtained considerable predictive skill in monthly means and extended-range forecasts, but their method did not yield any improvements at the 10-day time scale. Zheng et al. (2013) separated predictable components and unpredictable random components from the standpoint of error growth, and used this method to correct errors in the predictable components in extended-range forecasts, improving the forecast skill to some extent.

In summary, researchers have extensively developed the analog-dynamical method, which has improved the forecast at time scales longer than medium range. This improvement is due to the theoretical basis of the analog-dynamical method in long-range forecasts: the analog rhythm phenomenon, which is a nonuniform oscillation of analog deviation disturbance caused by nonlinear atmosphere–earth coupling and seasonal variation of monthly mean circulation (Huang and Chou 1990). External forcing and low-frequency flow patterns play leading roles at long-range time scales and the analog characteristics are evident. As for the medium-range forecast within 10 days, the role of the initial field is crucial and internal errors may grow nonlinearly. Therefore, it is difficult to parameterize state-dependent errors to improve forecast skill.

The purpose of the present study is to parameterize these state-dependent errors and improve model performance by reconsidering and developing the analog-dynamical method in an operational weather forecast system, on the basis of research of pioneer contributors. The dynamic model and dataset used in this study are introduced in the next section. The strategies and correction procedure are described in section 3. Section 4 lists the main verification statistics used to assess forecast skill. The main results of experiments are presented in section 5, and the results are summarized and discussed in the conclusions.

2. Dynamic model and data

The dynamic model used in this study is the Global/Regional Assimilation and Prediction System (GRAPES), which was developed by the China Meteorological Administration (CMA) in collaboration with several universities, and has been applied to operational forecasts. GRAPES has the following main characteristics: a fully compressible nonhydrostatic model core with a semi-implicit and semi-Lagrangian time integration scheme; a height-based terrain-following coordinate; longitude–latitude grid points with Arakawa C staggered arrangement for horizontal discretization; a Charney–Philips scheme for vertical discretization; free surface of a rigid body set as the top and bottom boundary conditions; physical schemes including cumulus convection, microphysics, radiation, planet boundary layer process, and earth surface processes; and code architecture modularized and parallelized with high flexibility. Details of this model have been reported by Chen et al. (2008) and Zhang and Shen (2008).

The global version of the model is chosen for correction because the spatial resolution of the global model is equal to that of the historical dataset. The horizontal resolution is set to 1° × 1° to avoid errors arising from interpolation between model grids and reanalysis data grids.

The NCEP Final (FNL) Operational Global Analysis data product is used as the initial field and the validator for the forecast. It has a global coverage with horizontal resolution of 1° × 1°, 26 vertical layers, and a 6-h temporal interval. Correspondingly, model outputs, including temperature, geopotential height, zonal wind, meridional wind, and humidity, are postprocessed at the same vertical level and output interval. The NCEP real-time global surface sea temperature (RTG_SST) analysis dataset is used to drive global GRAPES with a 1° × 1° horizontal resolution.

3. Strategy and correction procedure

In general, numerical weather prediction is proposed as an initial-value problem, and the evolution of model atmosphere can be described as the solution to the following Cauchy problems:

$$\frac{\partial \boldsymbol{\psi}}{\partial t} = \mathcal{L}(\boldsymbol{\psi}), \tag{1}$$

$$\boldsymbol{\psi}(\mathbf{x}, t)|_{t=t_0} = \mathbf{G}(\mathbf{x}), \tag{2}$$

where $\boldsymbol{\psi} \in \mathbb{R}^n$ is the model atmosphere state vector; n is the freedom degrees of the model; $\mathbf{G}(\mathbf{x})$ is the initial status, while $\mathbf{x}$ is a vector in the spatial coordinates; and $\mathcal{L}$ is the numerical model operator of $\boldsymbol{\psi}$, indicating the processes that the model can describe. The exact atmospheric state vector in $\mathbb{R}^n$ is expressed as $\boldsymbol{\varphi}$. The model error operator can be described as $\mathcal{E}(\boldsymbol{\varphi})$, which indicates the processes of the model do not consider or cannot be parameterized precisely, as a functional of $\boldsymbol{\varphi}$. By introducing this term, an accurate atmospheric model can be expressed as

$$\frac{\partial \boldsymbol{\varphi}}{\partial t} = \mathcal{L}(\boldsymbol{\varphi}) + \mathcal{E}(\boldsymbol{\varphi}), \tag{3}$$

$$\boldsymbol{\varphi}(\mathbf{x}, t)|_{t=t_0} = \mathbf{G}(\mathbf{x}). \tag{4}$$

The forecast error at a lead time of τ is given by

$$\begin{aligned}\mathcal{P}(\boldsymbol{\varphi}, \boldsymbol{\psi}, \tau) &= \boldsymbol{\varphi}|_{t=t_0+\tau} - \boldsymbol{\psi}|_{t=t_0+\tau} \\ &= \int_{t_0}^{t_0+\tau} [\mathcal{L}(\boldsymbol{\varphi}) + \mathcal{E}(\boldsymbol{\varphi})]\, dt - \int_{t_0}^{t_0+\tau} \mathcal{L}(\boldsymbol{\psi})\, dt.\end{aligned} \tag{5}$$

Assuming that the initial value error and computational error are not considered, the forecast error depends on $\mathcal{E}(\boldsymbol{\varphi})$. When the model is accurate, $\mathcal{E}(\boldsymbol{\varphi}) = 0$, and it can derive to $\mathcal{P}(\boldsymbol{\varphi}, \boldsymbol{\psi}, \tau) = 0$.

It can be proven given some hypotheses (see the proof in the appendix) that the functional $\mathcal{P}(\boldsymbol{\varphi}, \boldsymbol{\psi}, \tau)$ can constitute a continuous curved surface on $\mathbb{R}^n \times \mathbb{R}^n$, and the following theorem can be established:

$$\begin{gathered}\forall \varepsilon > 0,\ \boldsymbol{\varphi}_0 \in \mathbb{R}^n,\ \boldsymbol{\psi}_0 \in \mathbb{R}^n,\ \exists \delta > 0, \quad \text{whenever} \\ \boldsymbol{\varphi} \in \mathbb{R}^n, \boldsymbol{\psi} \in \mathbb{R}^n, \|\boldsymbol{\varphi} - \boldsymbol{\varphi}_0\| < \delta \quad \text{and} \quad \|\boldsymbol{\psi} - \boldsymbol{\psi}_0\| < \delta, \\ \text{such that} \quad \|\mathcal{P}(\boldsymbol{\varphi}, \boldsymbol{\psi}, \tau) - \mathcal{P}(\boldsymbol{\varphi}_0, \boldsymbol{\psi}_0, \tau)\| < \varepsilon.\end{gathered}$$

This is the continuity theorem of $\mathcal{P}(\boldsymbol{\varphi}, \boldsymbol{\psi}, \tau)$ on $\mathbb{R}^n \times \mathbb{R}^n$ about $\boldsymbol{\varphi}$ and $\boldsymbol{\psi}$. The schematic illustrating the continuity is shown in Fig. 1. Following this theorem, if there exists n historical reference states $\tilde{\boldsymbol{\varphi}}_1, \tilde{\boldsymbol{\varphi}}_2, \ldots\ldots, \tilde{\boldsymbol{\varphi}}_n$ in the δ neighborhood of $\boldsymbol{\varphi}_0$, and the corresponding model state vectors $\tilde{\boldsymbol{\psi}}_1, \tilde{\boldsymbol{\psi}}_2, \ldots\ldots, \tilde{\boldsymbol{\psi}}_n$ are in the δ neighborhood of $\boldsymbol{\psi}_0$, such that the forecast errors satisfy the following condition:

$$\|\mathcal{P}(\tilde{\boldsymbol{\varphi}}_k, \tilde{\boldsymbol{\psi}}_k, \tau) - \mathcal{P}(\boldsymbol{\varphi}_0, \boldsymbol{\psi}_0, \tau)\| < \varepsilon \quad (k = 1, 2, \ldots\ldots n). \tag{6}$$

This indicates that $\mathcal{P}(\boldsymbol{\varphi}_0, \boldsymbol{\psi}_0, \tau)$ can be interpolated by $\mathcal{P}(\tilde{\boldsymbol{\varphi}}_k, \tilde{\boldsymbol{\psi}}_k, \tau)$. In fact, $\boldsymbol{\varphi}$ can be regarded as a small disturbance superimposed on $\tilde{\boldsymbol{\varphi}}_k$ (i.e., $\boldsymbol{\varphi} = \tilde{\boldsymbol{\varphi}}_k + \Delta\boldsymbol{\varphi}_k$), where $\tilde{\boldsymbol{\varphi}}_k$ satisfies the exact atmospheric evolution:

$$\frac{\partial \tilde{\boldsymbol{\varphi}}_k}{\partial t} = \mathcal{L}(\tilde{\boldsymbol{\varphi}}_k) + \mathcal{E}(\tilde{\boldsymbol{\varphi}}_k), \tag{7}$$

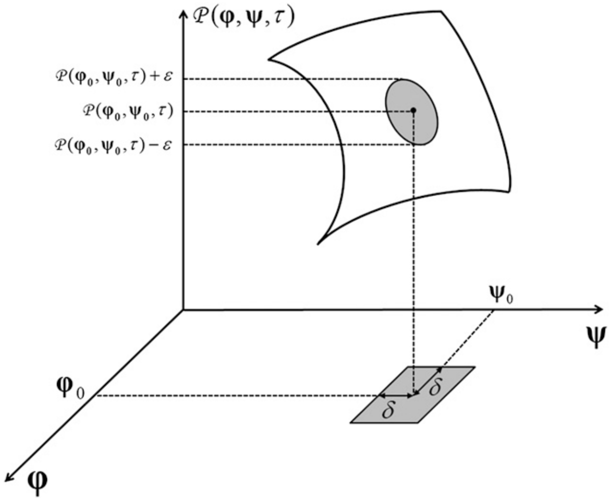

FIG. 1. Schematic illustrating the continuity of forecast error.

$$\tilde{\varphi}_k(\mathbf{x}, t)|_{t=t_1} = \tilde{\mathbf{G}}(\mathbf{x}), \tag{8}$$

where t_1 is the initial time of $\tilde{\varphi}_k$. The corresponding forecast error at the lead time of τ is

$$\begin{aligned}\mathcal{P}(\tilde{\varphi}_k, \tilde{\psi}_k, \tau) &= \tilde{\varphi}_k|_{t=t_1+\tau} - \tilde{\psi}_k|_{t=t_1+\tau} \\ &= \int_{t_1}^{t_1+\tau} [\mathcal{L}(\tilde{\varphi}_k) + \mathcal{E}(\tilde{\varphi}_k)]\, dt - \int_{t_1}^{t_1+\tau} \mathcal{L}(\tilde{\psi}_k)\, dt.\end{aligned} \tag{9}$$

From this perspective, the estimation of forecast errors can be converted to the interpolation of multivariate functions. Any special point on the curved surface can be interpolated by the points in the δ neighborhood, and their functional value differences would be less than ε. Thus, the current forecast error can be interpolated with the corresponding hindcast errors of some selected analog reference states. If n historical reference states exist in the delta neighborhood, the special forecast error can be interpolated by the corresponding n forecast errors. In extreme conditions, the control forecast corresponds to the neighborhood of $\delta = 0$ and no historical reference state is used. When the neighborhood extends to the entire $\mathbb{R}^n$ space, it corresponds to a systematic correction and the ensemble mean error of all the historical states in the space is obtained. Theoretically, interpolation in the neighborhood of limited δ provides more accurate results compared with the two situations above. This is the nature of the analog-dynamical method. The comparison between the practical effect of analog-dynamical methods, the control forecast and the systematic correction will be shown in the results section. In practice, the experimental correction scheme is as follows in the sections 3a–3c.

a. Step 1: Establishing the historical dataset

The FNL Operational Global Analysis data with a 6-h temporal interval from 2001 to 2010 were collected to establish the historical dataset, which is considered the reference state here.

b. Step 2: Historical analog search

From the proof of the above theorem (see the appendix), we can conclude that the following conditions should be satisfied to ensure the establishment of the continuity theorem:

1) Analog of initial value [i.e., $\|\mathbf{G}(\mathbf{x}) - \tilde{\mathbf{G}}(\mathbf{x})\| \ll \|\mathbf{G}(\mathbf{x})\|$];
2) Analog of boundary, by which state vectors of the current state and the reference state can have similar time evolutions; and
3) Limited lead time, which ensures that $\|\varphi - \tilde{\varphi}\|$ and $\|\psi - \tilde{\psi}\|$ will not grow larger over time.

The analog search should sufficiently consider the above three criteria. For criterion 1, the 500-hPa height field is selected as the analog variable for simplicity to search similar initial fields. The criterion used is the analog deviation (Li 1986), which is defined as

$$C_{ij} = \frac{\alpha R_{ij} + \beta D_{ij}}{\alpha + \beta}, \tag{10}$$

$$R_{ij} = \frac{1}{m} \sum_{k=1}^{m} |H_{ij}(k) - E_{ij}|, \tag{11}$$

$$D_{ij} = \frac{1}{m} \sum_{k=1}^{m} |H_{ij}(k)|, \tag{12}$$

$$H_{ij}(k) = H_i(k) - H_j(k), \tag{13}$$

$$E_{ij} = \frac{1}{m} \sum_{k=1}^{m} H_{ij}(k), \tag{14}$$

where R_{ij} is the pattern similar parameter, D_{ij} is the intensity similar parameter, and α and β are their contribution coefficients, setting $\alpha = 2$ and $\beta = 1$ in this study to emphasize the effects of patterns in the height field. Here $H_i(k)$ is the height field of sample i, and m is the total number of grids.

According to criterion 2, the search is limited to the same season and time of day as the current state to avoid the effects of seasonal and diurnal variations. For a global model, the external forcing of sea surface temperature

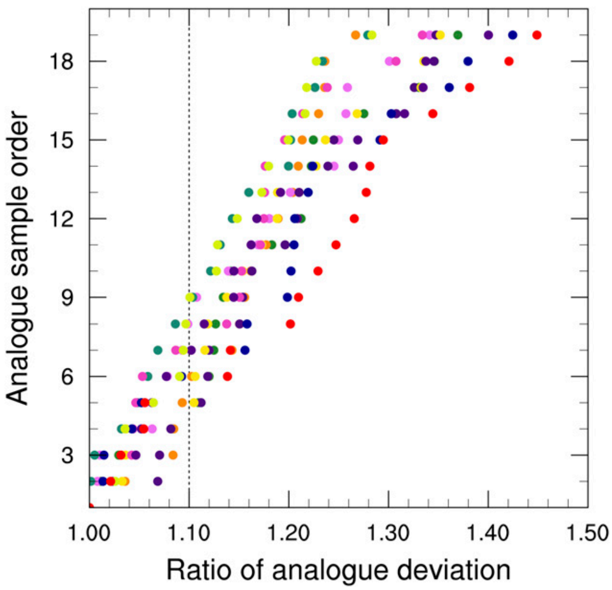

FIG. 2. Variance in analog deviation ratio by sample order. Each color represents a case, the y axis represents the analog sample order of each case, and the x axis is the corresponding analog deviation of each sample divided by the analog deviation of the first sample in the case.

(SST) is important, so the historical reference states are classified into three types by the Niño-3.4 index: El Niño type, La Niña type, and normal type. The search scope of the analog is limited to the corresponding type of the current initial field.

Criterion 3 illustrates that the persistence of the atmospheric analog is finite and the current forecast state will no longer be similar to the historical analog state selected with increasing lead time. Therefore, the historical analog states have to be updated again. The update period is set at 5 days, which is the general period of the large-scale flow regime. The forecast restarts after each period.

Theoretically, the more analogs are used, the more improvement can be made. According to the continuity theorem, when ε is fixed there is a δ neighborhood for any forecast state whose distance to the current state is less than δ, such that the corresponding distance of these two forecast errors would be less than ε. In practical situations, it is difficult to ensure that all the selected reference states are in this δ neighborhood. As a result, the quality of reference states determines the correction effect. Because the historical datasets used are from 2001 to 2010 and the volume is not large enough, it is difficult to ensure the quality of analogs when too many samples are selected. Using analog deviation to describe the analog quality, the values of the analog deviation of each sample divided by the analog deviation of the most similar samples of the case are shown in Fig. 2. As shown in the figure, the analog quality decreases as the sample order increases. When the analog sample order is lower than four, most of the ratios are less than 1.1. Previous research about monthly forecasts (Ren and Chou 2007) has shown that four analogs offer effective correction, so in this situation, we select four analog samples for each case.

Based on the above principle, the procedures for selecting analogs are as follows. First, the analog selection is restricted to the same season and time of day as the current initial field. Second, because the Niño-3.4 index is calculated by month, the selection is limited to months with the same SST type as the current state. Third, the most similar sample is searched using the analog deviation in each satisfied month. The selected samples are then sorted by analog deviation and the first four similar samples are selected. The reason for not calculating the best analogs over the set is to avoid the intensive distribution of the selected samples in some continuous period. In that case, these samples would have a similar correction effect. To enhance the representativeness, the samples are selected by month.

c. *Step 3: Forecast error correction*

Both online correction and after-the-fact correction can be considered. Because online correction may produce additional errors and influence the balance between different physical quantities, the after-the-fact method is used here to avoid disrupting dynamic coordination. The frequency of correction is limited to the interval of historical reference states, and the forecast error estimation from multiple historical analog states is corrected after the fact in the intervals.

These steps of the experimental scheme are illustrated by the flow diagram in Fig. 3. First, parameters such as the correction interval and analog update period are defined. Based on the current initial field, some analog samples are selected from the historical dataset. When the current forecast is conducted, the corresponding hindcasts are also performed and we can determine the hindcast errors at each correction interval. The ensemble mean of these errors is taken as the correction estimation to be added to the current forecast output. This correction is conducted after the fact and will not affect the next forecast. When the time arrives for the analog update period, the corrected forecast is taken as the initial field to reselect analog samples in the historical datasets to rerun the above procedures, until the current forecast is finished. Additionally, because the assimilation model is different from the forecast model, an initialization using a digital filter (Lynch and Huang 1992) is performed before the current forecasts and historical hindcasts are conducted to filter high-frequency gravity

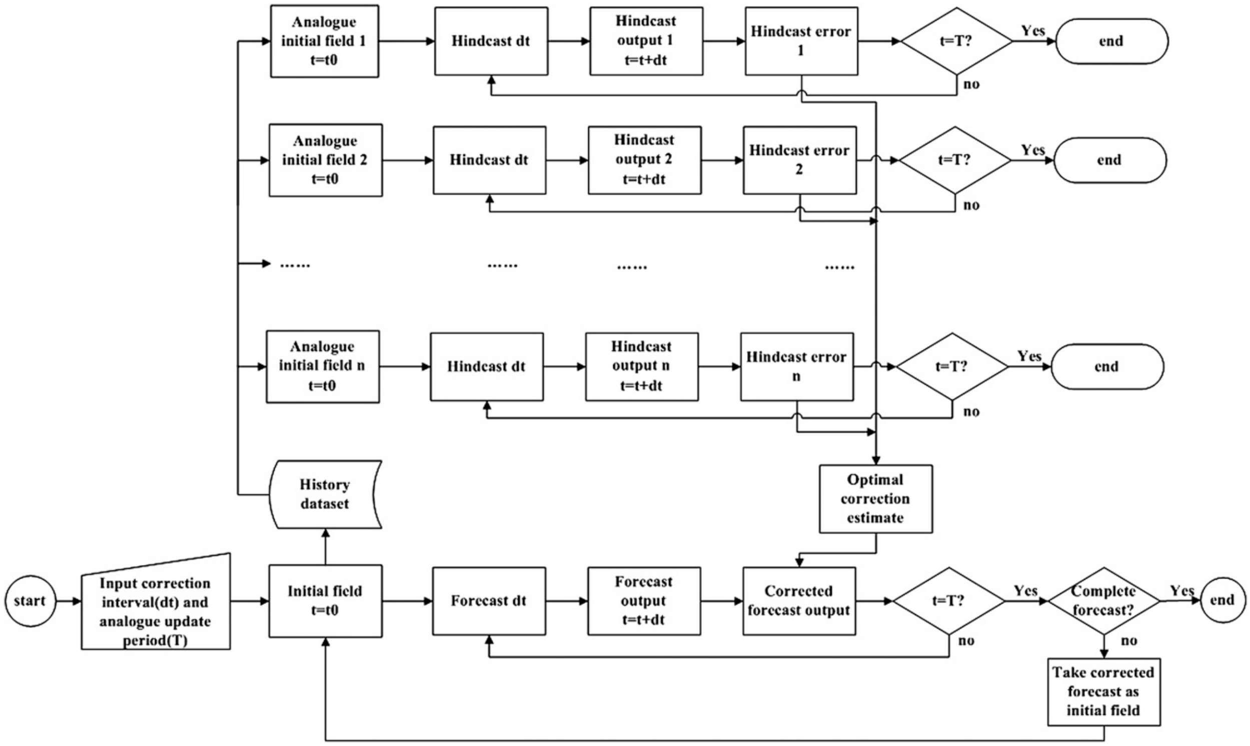

FIG. 3. Flow diagram illustrating the correction procedure.

waves and make the initial field adaptive to the GRAPES model.

Following this strategy, 40 independent cases with 10-day integrations are randomly selected from summer (June–August) and winter (December–February) of 2011. The effects of the analog correction are assessed in the results section.

4. Verification statistics

The verification statistics used to assess the predictive skill of 10-day integrations for control and correction forecasts are presented below.

a. Anomaly correlation coefficient (ACC)

The ACC of latitude j is

$$\mathrm{ACC}(j)=\frac{\sum_{i=1}^{N_j}\left[F_{ij}-C_{ij}-\frac{1}{N_j}\sum_{i=1}^{N_j}(F_{ij}-C_{ij})\right]\left[A_{ij}-C_{ij}-\frac{1}{N_j}\sum_{i=1}^{N_j}(A_{ij}-C_{ij})\right]}{\sqrt{\sum_{i=1}^{N_j}\left[F_{ij}-C_{ij}-\frac{1}{N_j}\sum_{i=1}^{N_j}(F_{ij}-C_{ij})\right]^2\sum_{i=1}^{N_j}\left[A_{ij}-C_{ij}-\frac{1}{N_j}\sum_{i=1}^{N_j}(A_{ij}-C_{ij})\right]^2}}, \qquad (15)$$

where F_{ij} is the forecast value, A_{ij} is the analysis value, C_{ij} is the climate-mean value, and N_j is the number of grids at latitude j. Considering the weighted mean, the global ACC is

$$\mathrm{ACC}=\frac{\sum_{j=1}^{N}\mathrm{ACC}(j)\cos\theta_j}{\sum_{j=1}^{N}\cos\theta_j}. \qquad (16)$$

The ACC reflects pattern correlation between forecasted and analyzed anomalies, which can be used to assess the errors in position and strength of flow regimes.

b. Root-mean-square error (RMSE)

The RMSE of latitude j is

$$\mathrm{RMSE}(j)=\sqrt{\frac{1}{N_j}\sum_{i=1}^{N_j}(F_{ij}-A_{ij})}, \qquad (17)$$

where F_{ij} is the forecast value, A_{ij} is the analysis value, and N_j is the number of grids at latitude j. Considering the weighted mean, the global RMSE is

$$\mathrm{RMSE} = \frac{\sum_{j=1}^{N} \mathrm{RMSE}(j)\cos\theta_j}{\sum_{j=1}^{N} \cos\theta_j}. \tag{18}$$

The RMSE reflects the mean degree of forecast departure from the analysis field.

c. Kinetic energy

Kinetic energy is an effective diagnostic measure to characterize atmospheric circulation. In this study, it is used to assess the correction ability. The zonal-averaged mean kinetic energy can be decomposed as follows (Jung 2005):

$$K = K_{\mathrm{SMTM}} + K_{\mathrm{SMTE}} + K_{\mathrm{SETM}} + K_{\mathrm{SETE}}, \tag{19}$$

$$K = \frac{1}{2}(\overline{[u \times u]} + \overline{[v \times v]}), \tag{20}$$

$$K_{\mathrm{SMTM}} = \frac{1}{2}([\overline{u}] \times [\overline{u}] + [\overline{v}] \times [\overline{v}]), \tag{21}$$

$$K_{\mathrm{SMTE}} = \frac{1}{2}(\overline{[u]' \times [u]'} + \overline{[v]' \times [v]'}), \tag{22}$$

$$K_{\mathrm{SETM}} = \frac{1}{2}([\overline{u}^* \times \overline{u}^*] + [\overline{v}^* \times \overline{v}^*]), \tag{23}$$

$$K_{\mathrm{SETE}} = \frac{1}{2}(\overline{u'^* \times u'^*} + \overline{v'^* \times v'^*}), \tag{24}$$

where brackets denote a zonal mean, asterisks denote departures from the zonal mean, overbars denote the temporal mean, and primes denote departures from the temporal mean. The variable K_{SMTM} is the zonal long-term mean term, which reflects the climatic zonal mean; K_{SMTE} is the transient zonal mean term, which reflects the temporal variation of zonal mean flow; K_{SETM} is a stationary eddy term, which reflects the permanent atmospheric action center and the impacts of ocean–land distribution and topography; and K_{SETE} is transient eddy term, reflecting synoptic-scale systems.

5. Results

The mean results of 40 independent cases are presented in this section. The general correction effect is discussed first using the verification statistics of the ACC and RMSE. Figure 4 shows the correction results of the 500-hPa height field by forecast time. The global result shows that the correction has a positive effect at all lead times and the period of validity is extended from 6.7 to 7.5 days. The improvement is significant beyond 5 days as the control model has a relatively high predictive ability within 5 days, with the maximum improvement reaching 0.06 at the 10th day. The shaded bands indicate that the variance in ACC by cases becomes larger with the increase of lead time. Because the initialization is conducted using a digital filter, as mentioned above, and interpolation is conducted because of the inconsistency of horizontal grids between the forecast output and FNL data, the ACC starts at less than 1. The results in the extratropical Northern Hemisphere (NH), extratropical Southern Hemisphere (SH), and tropics are also shown to explore the correction effect independently. The NH (20°–80°N) result reveals that the correction effect appears at all lead times and increases with the lead time. In the SH (20°–80°S), the uniform underlying surface makes the skill of the control forecasts relatively high, and the correction effect is not as obvious as in the NH, especially during the first 5 days. The most evident improvement appears in the tropics (20°S–20°N), and the corresponding period of validity is extended by approximately 1.25 days. The reason for this may be that the forecast errors in the tropics are more associated with subgrid-scale parameterization, which exhibit systematic characteristics that can be captured by the correction. To clearly demonstrate the correction effect and variation among different cases, Fig. 5 shows the global mean relative improvements of ACC and corresponding error bars with 95% confidence intervals. As shown in the figure, relative improvements increase with the lead time. Meanwhile, uncertainty also increases with lead time, indicating that the correction is state dependent and relies strongly on the initial field.

To explore the vertical structure of correction ability, ACC and RMSE values are calculated in global height fields at all levels, as shown in Fig. 6. Meanwhile, to compare the analog-dynamical correction with the two extreme conditions mentioned in section 3, a systematic correction is conducted by adding the climate drift, which is the ensemble mean of 5-day hindcast errors from 2001 to 2010 considering seasonal changes. The procedures of systematic correction are as follows: the 6-h hindcast error can be denoted as $\delta\varphi_6$, which is the bias of 6-h hindcast from analysis data, and the ensemble mean of $\delta\varphi_6$ is given by $\overline{\delta\varphi_6} = (1/N)\sum_{i=1}^{N}\delta\varphi_6(i)$, where N = years × days in a season × 6-h intervals [i.e., for summer (June–August), $N = 10 \times (30 + 31 + 31) \times 4$]. The 5-day mean hindcast errors with 6-h intervals $\overline{\delta\varphi_6}, \overline{\delta\varphi_{12}}, \overline{\delta\varphi_{18}}, \ldots, \overline{\delta\varphi_{120}}$ are calculated in the same way.

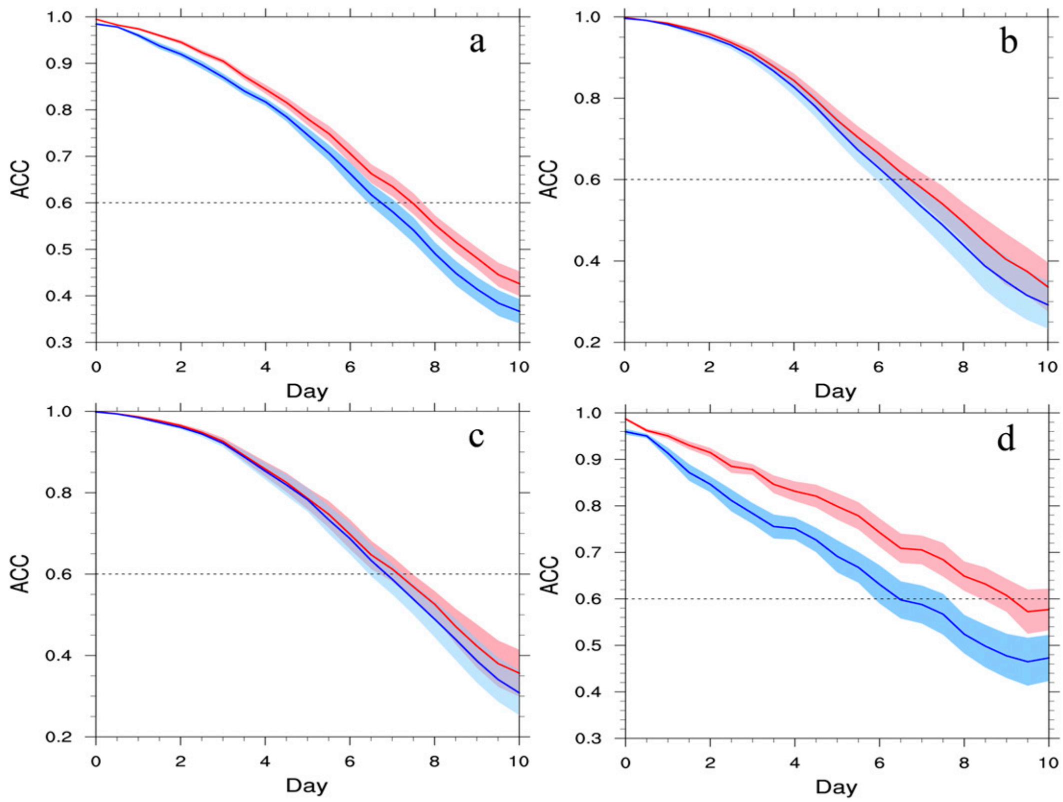

FIG. 4. Mean ACC of the global 500-hPa height field between the forecast and analysis data as a function of forecast time for the control forecast (blue) and corrected forecast (red) in different regions: (a) global, (b) extratropical Northern Hemisphere (20°–80°N), (c) extratropical Southern Hemisphere (20°–80°S), and (d) tropics (20°S–20°N). The shaded bands indicate 95% confidence intervals.

These ensemble mean estimations are used to make posteriori bias corrections to the 5-day control forecast. The model is restarted after 5 days with corrected forecast outputs, and the posteriori bias corrections are repeated with the new estimates. For the current forecast in winter, the procedures are the same, using the hindcasts of December–February from 2001 to 2010. The ACC results indicate that systematic correction causes a positive improvement only at the upper and lower levels with a lead time of 5 days. This may be associated with the parameterizations of the land surface, boundary layer, and stratosphere, which exhibit systematic characteristics. In contrast, the analog-dynamical forecast is improved at all levels. With the 10-day lead time, positive improvement is uniformly distributed among vertical levels in both corrections. The mean ACC increase in the systematic correction is 0.03, while that in the analog-dynamical forecast is 0.07. The maximum error reflected by the RMSE appears at 250 hPa. This may be related to weak simulation of the interaction between the tropopause and the stratosphere. The correction has a less obvious effect on the RMSE at the lead time of 5 days. The systematic correction makes the RMSE increase, while the analog-dynamical forecast has a positive effect at all levels, reducing it by 4 gpm on average. The correction effect becomes considerable with a 10-day lead time. Correction of the analog-dynamical forecast becomes significant as the level increases, reaching a maximum at 12 gpm and then decreasing, while a systematic correction effect is still not evident.

To further investigate the forecast skill and correction effect at different spatial scales, the forecast height field at 500 hPa is zonally expanded into Fourier series. The sum of the zero to third wave terms represents planetary-scale systems, and synoptic-scale systems are represented by the sum of fourth to ninth wave terms. The correction results for a planetary scale are shown in Figs. 7a,c. The ACC-indicated improvement in analog-dynamical results compared to the control result is remarkable, extending the period of validity from 7.5 to 8.6 days and raising the ACC at the 10-day forecast period by 0.1. A systematic correction effect is not evident, especially in the first 5 days, and the corresponding

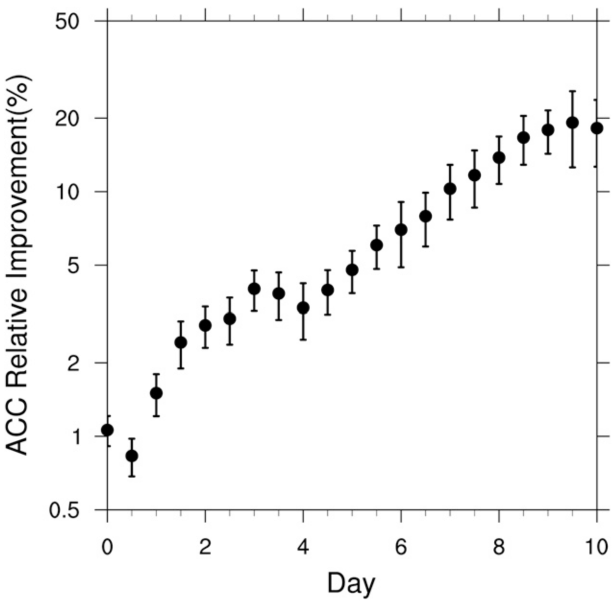

FIG. 5. Mean relative improvement of the ACC of global 500-hPa height field between the forecast and analysis data as a function of forecast time. The error bars represent 95% confidence intervals.

period of validity is 7.8 days. Analog-dynamical corrections reduce the RMSE at all lead times as shown in Fig. 7c, and are superior to the control forecast. Meanwhile, systematic correction yields no improvement. At the synoptic scale, neither correction has an effect at any lead time, as shown in Figs. 7b,d. This may be attributed to two factors. First, analog selection cannot accurately capture the synoptic-scale pattern and fails to capture the evolution of synoptic-scale errors. Second, either correction may introduce some noise, which has a similar scale to the synoptic systems, offsetting the positive correction effect. In other words, the improvement of analog-dynamical results is most often the result of corrections in planetary waves.

The above results reveal general improvement in the analog-dynamical method in terms of verification skill. As RMSE only reflects the mean bias, we investigated the bias distribution of the original model and compared it with the analog-dynamical corrected result. Figure 8 presents the zonal averaged 10-day forecast errors of the original forecast and the analog-dynamical forecast. The temperature results reveal that the original forecast is too cold for the stratosphere and too warm for lower levels at high latitudes in the SH. The height field in the original forecast is overestimated at the Antarctic and underestimated at high levels in the NH. Reverse pattern relationships appear between the original forecast and the correction. The correction rightly offsets high biases so that zonal-averaged errors are strongly weakened. It also indicates that both temperature and height fields are overcorrected in some regions, especially at high latitudes in the NH.

The horizontal distributions of forecast bias are shown in Figs. 9 and 10. Figure 9 shows that the forecast bias of height field has systematic features. Because the convergence of the spherical polar coordinates may cause instability in the calculation, the accuracy of the control forecast is weak and the height field is too high in the Antarctic. The forecast bias in the NH is affected by the land–ocean distribution, and high value areas are mainly distributed across the continent. This may be associated with the complex topography and defective land surface

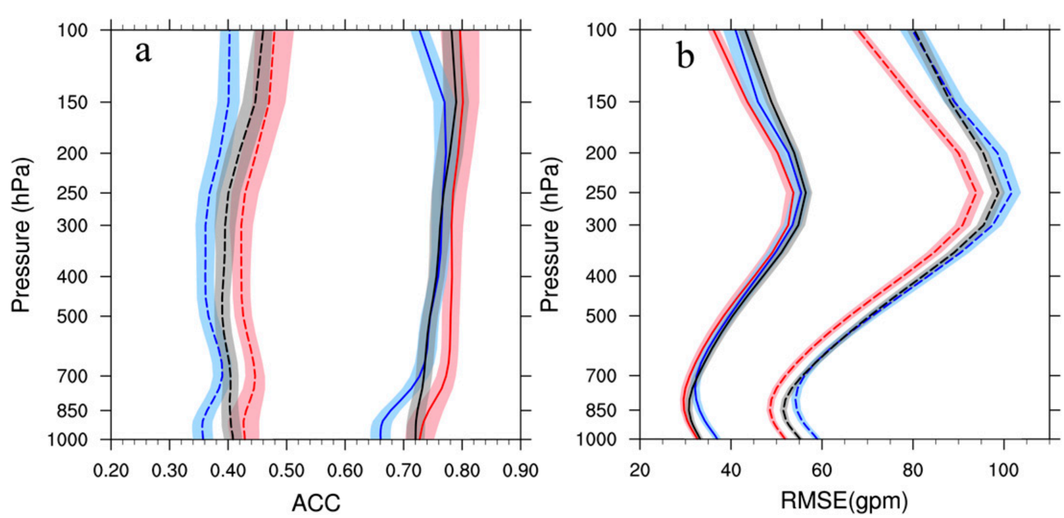

FIG. 6. Vertical distribution of the (a) ACC and (b) RMSE of global height field between forecast and analysis data for the control forecast (blue), systematic correction (black), and analog-dynamical forecast (red) at the forecast time of 5 (solid) and 10 (dashed) days, with shaded bands indicating 95% confidence intervals.

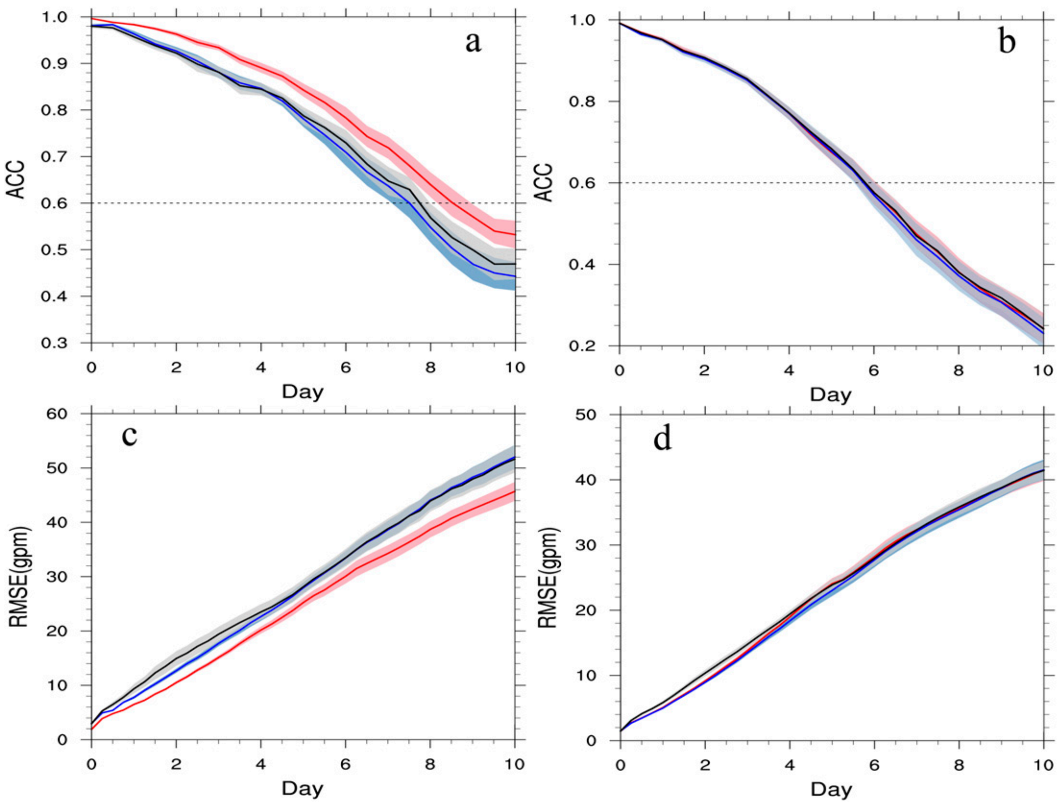

FIG. 7. ACC and RMSE of 500-hPa height field between forecast and analysis data depending on the spatial scale as a function of lead time for the control forecast (blue), analog-dynamical forecast (red), and systematic correction (black) for (a),(c) planetary-scale waves and (b),(d) synoptic-scale waves, with shaded bands indicating 95% confidence intervals.

parameterization. Overestimations are concentrated over Asia and North America at 850 hPa, and these regions are inversely underestimated at 500 hPa, matching the cold bias shown in Fig. 8. Less forecast bias appears for the tropics, where the magnitude of the height field is low and the ocean cover is large. The forecast bias reveals wave train characteristics at midlatitudes in both hemispheres, and is more evident in the SH with a zonal wavenumber of 5. Interestingly, the patterns of the wave train at 500 and 850 hPa are similar, indicating that the forecast errors on synoptic scales have a barotropic structure. This may be caused by the low temperature gradient due to the uniform sea surface. The correction exactly identifies the main area of errors and offsets biases, especially over the Antarctic and continents in the NH. However, overcorrection occurs in some areas at high and midlatitudes. The wave train still has a low magnitude and inversed phase, which is consistent with the weak correction effect on synoptic scales, as shown in Fig. 7.

Figure 10 illustrates the horizontal distributions of temperature forecast bias. An underestimation appears in the NH over the continent at both 500 and 850 hPa, with a maximum in North America, indicating that this is a systematic model error. The error may be caused by problems in the interaction between clouds and radiation of the model, resulting in error of the radiation budget. The magnitude of error at 850 hPa is greater than that at 500 hPa; this difference may arise from the land surface and boundary layer parameterizations, which are the most difficult schemes in the model. The model may also lack coordination between the land surface and boundary layer parameterizations, which could be overcome or lessened by careful diagnosis and debugging. In the SH, the forecast bias is not as evident at low and midlatitudes because the underlying surface of the ocean makes the temperature predicable over a longer period. An overall warm estimation appears at high latitudes of 500 and 850 hPa, especially over the Antarctic. The correction can exactly identify and offset the distribution characteristics of the warm bias. After the correction, the original errors are greatly decreased, as seen over continents in the NH. The corrected field has a narrow error range, with the maximum less than

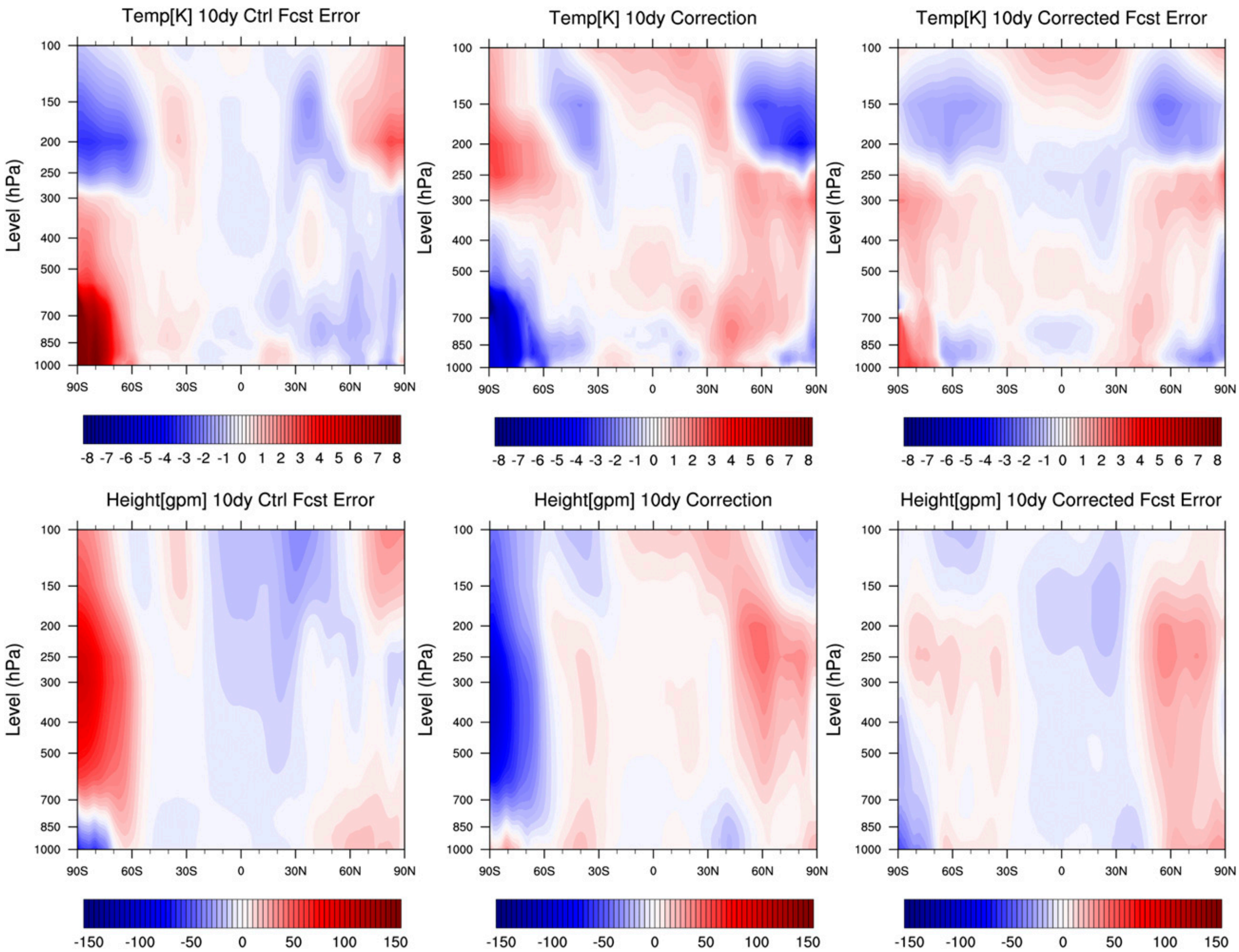

FIG. 8. Zonally averaged 10-day forecast errors for (left) global temperature field and height field of the control model, (middle) correction quantity by the analog-dynamical method, and (right) forecast errors after correction.

4 K at 850 hPa. However, the warm bias in the Antarctic is undercorrected, leaving a weak warm bias at both 500 and 850 hPa.

In addition to these thermodynamic quantities, improvements in the flow field need to be diagnosed. Kinetic energy is used here to characterize this effect. Figure 11 presents the forecast errors of kinetic energy for 6–10 days, along with the structure of corresponding reanalysis results from FNL data. The mean total kinetic energy is decomposed into four parts as described above, and each part is clearly shown. Notably, K_{SMTM} dominates the area of the subtropical jet streams. The largest errors appear in the upper-level jet area, with underestimations up to $80\,\mathrm{m}^2\,\mathrm{s}^{-2}$. They are inversely offset, with the error range reduced by half. K_{SETM} reflects the contribution of stationary waves and is most remarkable in mid- and upper levels of the atmosphere, corresponding to the atmospheric active centers. According to the results of the control model, it is obvious that this underestimation is concentrated in high value areas. These errors are reduced to some extent, but some underestimation still appears, up to $25\,\mathrm{m}^2\,\mathrm{s}^{-2}$. The transient terms include K_{SMTE} and K_{SETE}. The former reflects the temporal variations in zonal mean flow, such as the seasonal transform and index cycle, which is evident in the mid- and high latitudes. K_{SMTE} has a small magnitude because it is a slowly changing variable in 10-day forecasts. As a result, the original errors and correction are both small, and the range is decreased by half. K_{SETE} represents transient eddies and is the term of most concern. As a measure of the performance of baroclinic instability, its distribution is concentrated in midlatitude areas. The distribution of K_{SETE} errors is similar to the distribution of the values themselves, and the maximum underestimation is $90\,\mathrm{m}^2\,\mathrm{s}^{-2}$. Correction can effectively reduce the error to a certain extent, up to $20\,\mathrm{m}^2\,\mathrm{s}^{-2}$. Above all, the control forecast underestimates the kinetic energy, and correction can improve the forecast

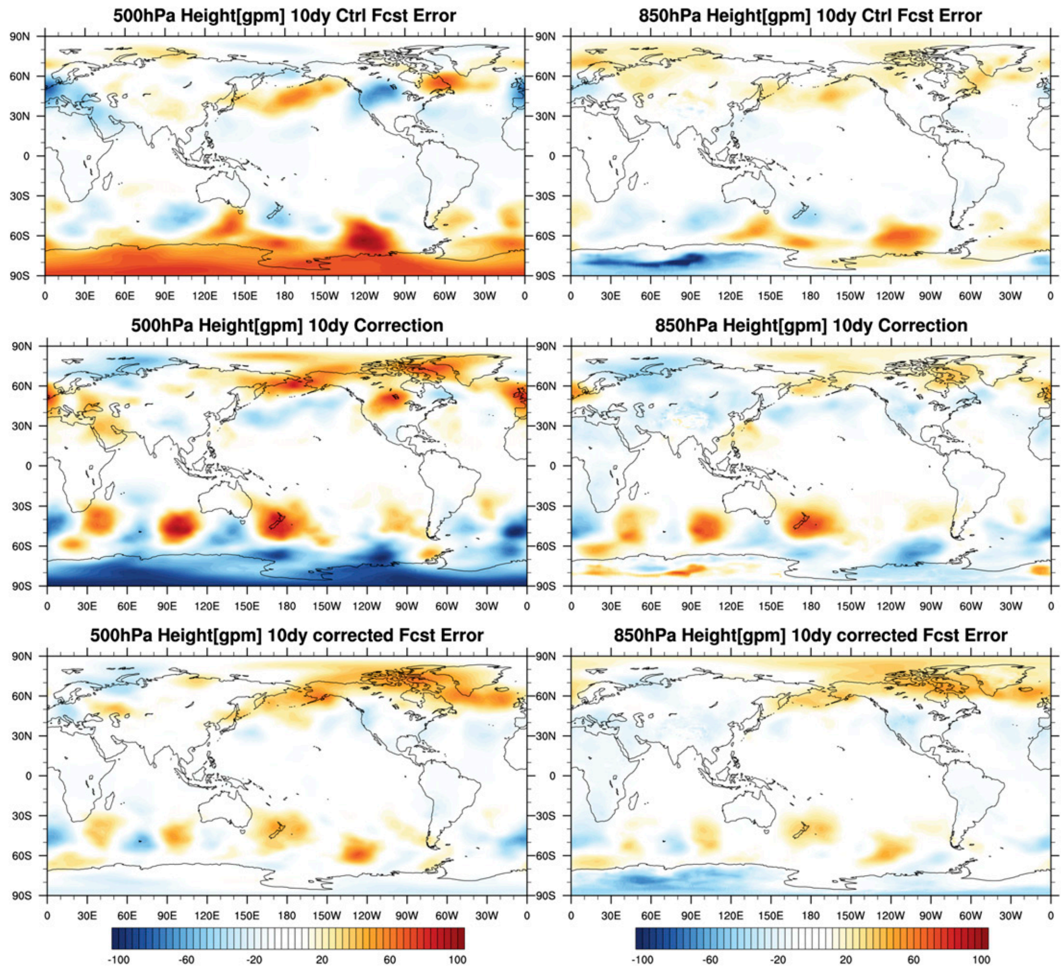

FIG. 9. Mean 10-day forecast errors for the global height field of (left) 500 hPa and (right) 850 hPa for (top) control model, (middle) correction by the analog-dynamical method, and (bottom) forecast errors after correction.

skill to some extent. However, the kinetic energy error is undercorrected and also underestimated after correction, at about half of the original magnitude.

6. Conclusions and discussion

Model deficiencies can be attributed to the model grid resolution not being sufficiently fine and the parameterizations not exactly describing subgrid-scale physical processes (e.g., those related to deficiencies in the dynamical framework, the land surface, and boundary layer parameterizations, etc., as discussed in the results section). The general approach to reducing systematic errors is to develop a model with more elaborate parameterizations and denser grid resolution. However, no matter how fine the model becomes, considerable systematic errors will still appear. Therefore, new forecast strategies are needed to correct for model errors by incorporating historical data, which include vast samples and may provide some information about model errors. However, because the atmosphere is a nonlinear system, it may not be efficient to use a large amount of historical data to establish statistical relationships between model errors and state variables. Analogs may be a useful alternative method.

This article presented an analog-dynamical method, based on the work of pioneer contributors and investigators, to correct a medium-range weather forecast system. The method is easy to operate and transport to other sophisticated models, so it may be appropriate for operational use, which is the objective of this work. The ensemble mean of hindcast errors from the historical analog samples is used to estimate current forecast error. The proof for continuity of forecast error provides theoretical support for this method. Based on the results of 40 randomly selected cases, we can conclude that the correction improves forecast skill and that the effect is increasingly significant with increased lead time. We also

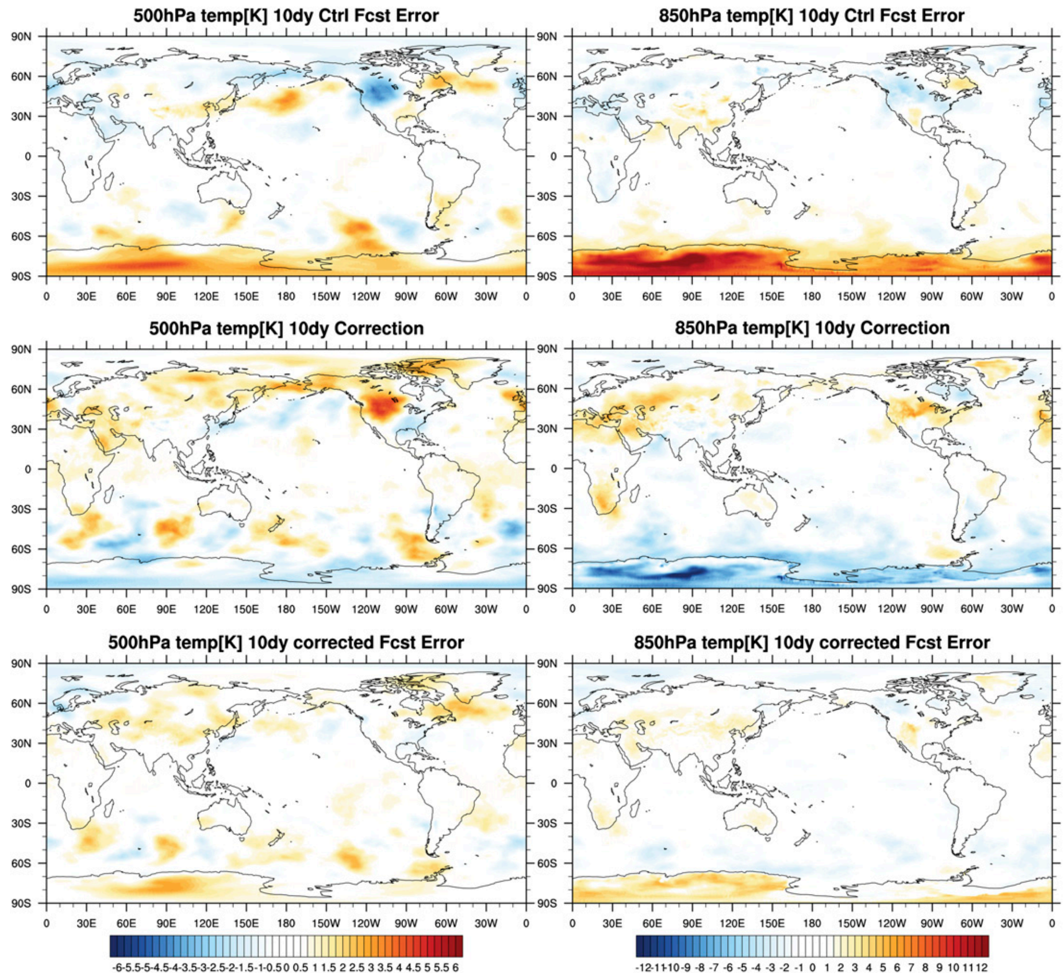

FIG. 10. As in Fig. 9, but for the temperature field.

confirmed that the improvement is superior to control and systematic corrections, and is mostly caused by corrections on planetary scales. Meanwhile, the improvement is stable at different altitudes. The biases of errors for pressure and temperature are greatly weakened with inverse correction, and kinetic energy is also modified to some extent. These findings demonstrate that the analog-dynamical method can capture the main characteristics of error pattern. The error magnitude of slowly changing variables, such as thermodynamic quantity, is appropriately estimated in these corrections. However, for rapidly changing variables such as kinetic energy, the estimation of error magnitude is narrowed, especially at energy of transient eddies.

Despite its improvements, the model still has some limitations. First, the method may introduce some additional errors. This is because the analog-dynamical correction is essentially an interpolation in $\mathbb{R}^n$ space, and the interpolation error is considerable when model errors are reduced to a certain degree. In this sense, interpolation errors strongly rely on the quality of selected analog samples, which is why careful selection of analog samples is required: we used only four samples for each case. Second, we empirically determined the amount of analog samples for each case and analog criteria. These will vary by model and dataset, so the optimal scheme should be confirmed by conducting numerical experiments. Third, FNL data are regarded here as the evolution of the real atmosphere, and used to validate the forecast and establish historical reference states, which will make the GRAPES behave like the FNL data. The findings presented here would be more convincing if an independent dataset was used for verification.

The analog update period is set at 5 days, which is the general period of the large-scale flow regime. Because analogs will diverge from each other more quickly on smaller spatial scales, the effects of shorter periods should also be verified. For comparison, the same scheme with update periods of 6, 12, 24, 60, and 120 h was used, and the average results of six cases are shown in Fig. 12. The

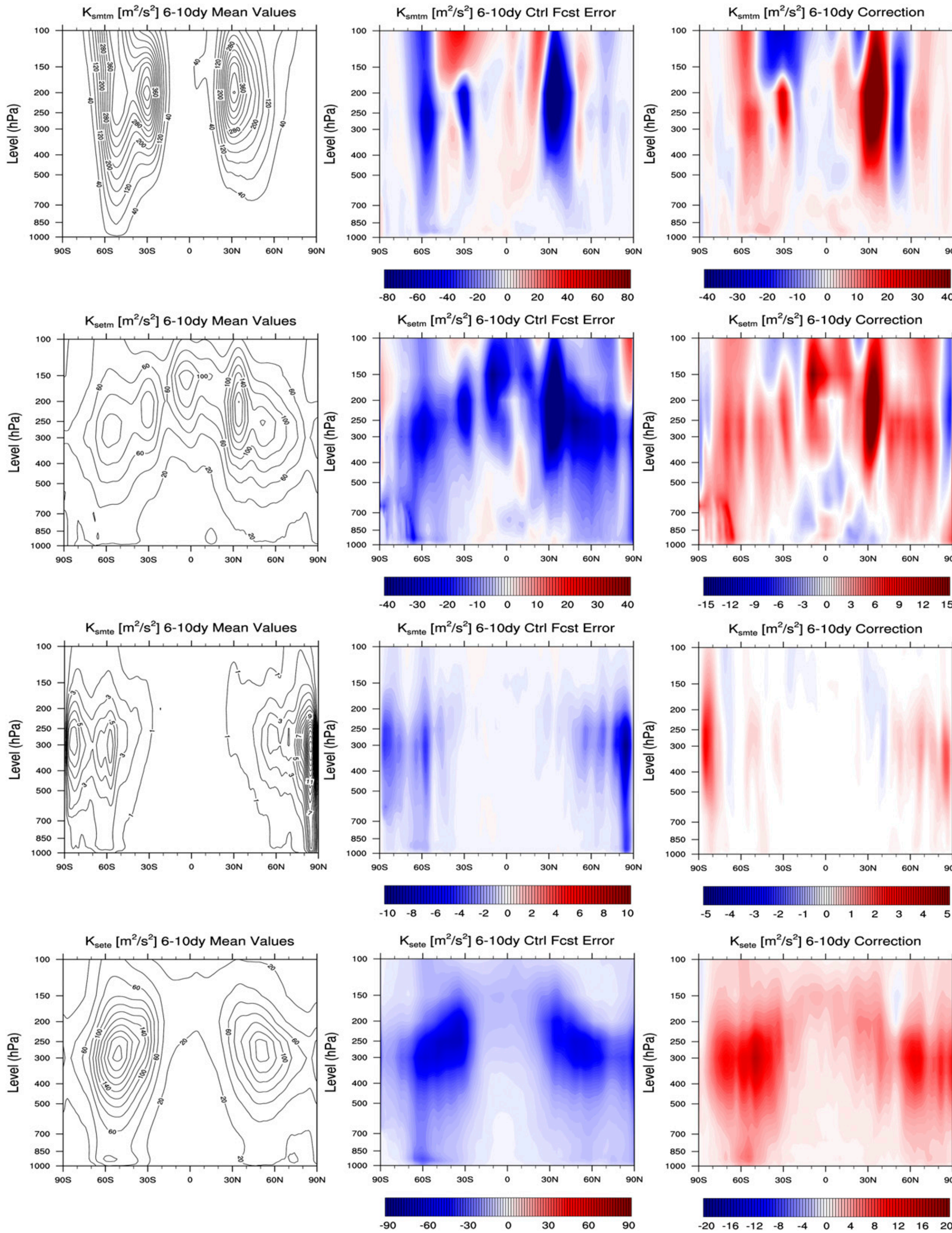

FIG. 11. Mean forecast errors around the four parts of the 6–10-day forecast kinetic energy for the (middle) control model and (right) analog-dynamical correction quantity. (left) The corresponding mean values from the FNL reanalysis data are also shown.

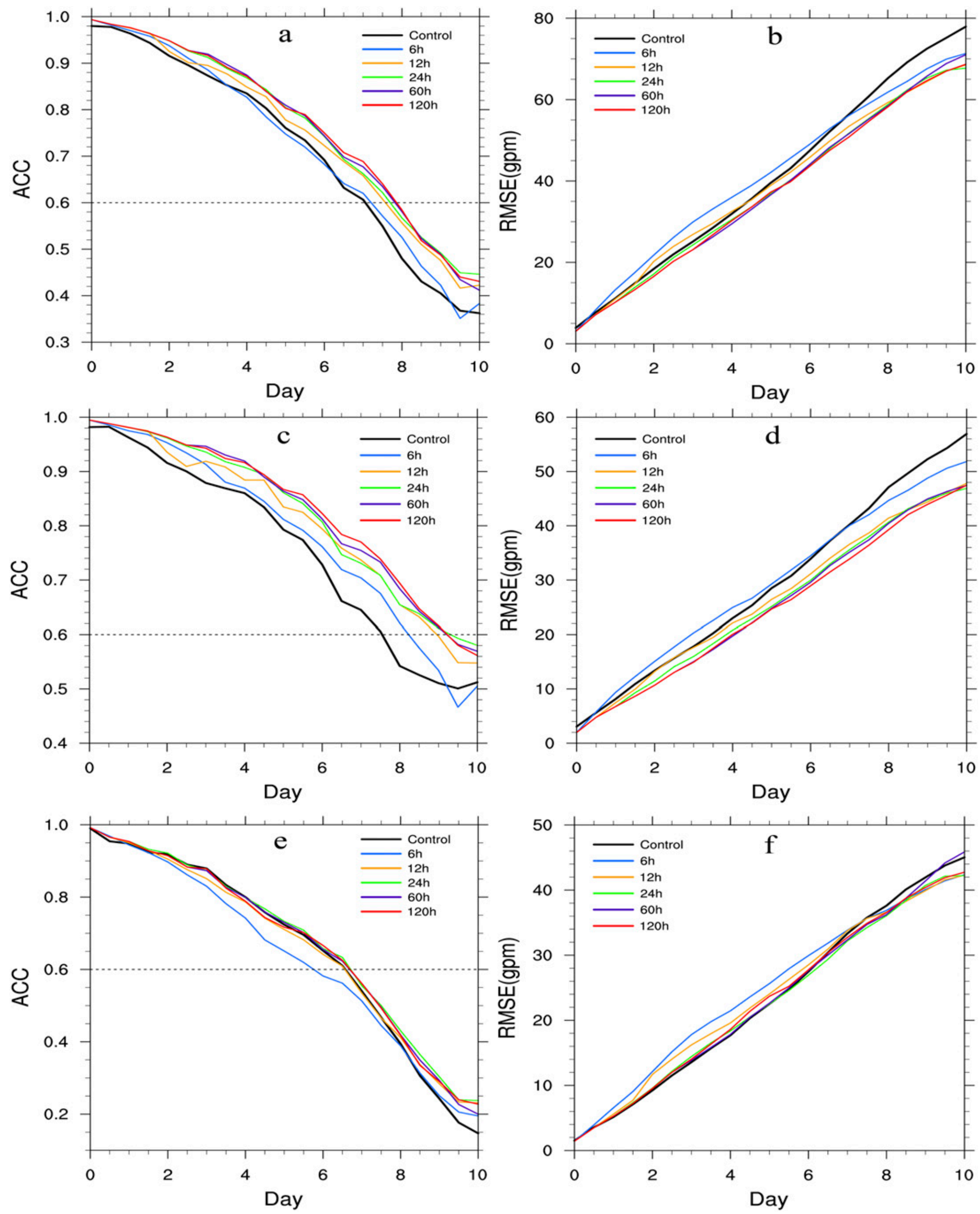

FIG. 12. Comparison of different analog update periods for the ACC and RMSE of the global 500-hPa height field between the forecast and analysis data depending on the spatial scale: (a),(b) all waves; (c),(d) planetary-scale waves; and (e),(f) synoptic-scale waves.

results demonstrate that the shortening of the update period presents no advantage, and the 6-h period worsens the effect for all waves. The reason for this may be that the forecast error is low at 6 h, and the positive effect of the correction may have the comparative magnitude of the noise it introduces. Only when the correction effect surpasses the noise will improvement be possible. The forecast skill is not sensitive to variations in the update period at 24, 60, and 120 h. None of the periods obviously improve the synoptic-scale waves, and all the corrections have a similar effect as the control forecast, except that the 6-h period causes the results to decline. For planetary-scale waves, most corrections can improve the forecast skill, and

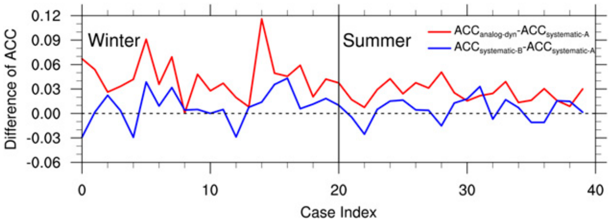

FIG. 13. Variance in the difference of ACC (red line: analog-dynamical forecast minus systematic-A forecast; blue line: systematic-B forecast minus systematic-A forecast) of 5-day forecast global 500-hPa height field by different cases. The x axis represents the 40 cases selected. The indexes of 0–19 are from winter (December–February) of 2011, and the indexes of 20–39 are from summer (June–August) of 2011.

120 h yields a slight advantage over others. In short, 5 days is an optimal update period that not only yields the most improvement, but also saves computation time.

The systematic correction used for comparison in this study is conducted by adding the ensemble mean hindcast errors from 2001 to 2010 considering seasonal changes, which is referred to as Systematic-A hereafter. To reduce the uncertainties in the difference between analog-dynamical correction and systematic correction, we conducted another method of systematic correction using the mean bias from the same month of previous year (Systematic-B hereafter). The ACC of global 500-hPa height field at the lead time of 5 days is calculated for each method (Systematic-A, Systematic-B, and analog-dynamical correction) and each case. For the convenience of comparing, the ACC of Systematic-A is subtracted from the ACC of Systematic-B and analog-dynamical correction, as shown in Fig. 13. The result indicates that the correction effect of Systematic-B is similar with that of Systematic-A. The analog-dynamical method is superior to both the two systematic corrections for almost all of the cases, especially for the cases in winter.

We can conclude that the analog-dynamical method demonstrates active performance in reducing biases in low-frequency systems. Future research should focus on improvements for time-varying planetary waves and Rossby waves, which may be associated with the nonlinear growth of internal errors. Online analog-dynamical correction is considered to reduce cumulative nonlinear growth of state-dependent bias, and will be investigated and presented in a future paper.

Acknowledgments. This research is supported by the Special Scientific Research Project for Public Interest (GYHY201206009), National Key Technology Research and Development Program (2009BAC51B04), and National Natural Science Foundation of China (41105070). The computing in this project is conducted at the Gansu Computing Center. The authors thank Carolyn Reynolds, Shujuan Hu, Chaojiu Da, Haile Xue, Fabio D'Andrea, Litai Kang, and three anonymous reviewers for their valuable comments and helpful suggestions on this research. The authors also thank the Numerical Weather Prediction Center of China Meteorological Administration for providing the GRAPES model and for kind guidance on its implementation.

APPENDIX

Proof of the Continuity Theorem Regarding Forecast Error

For any exact atmosphere state vector $\boldsymbol{\varphi} \in \mathbb{R}^n$ and model atmosphere state vector $\boldsymbol{\psi} \in \mathbb{R}^n$, the forecast error $\mathcal{P}$ at a lead time of τ is given by

$$\mathcal{P}(\boldsymbol{\varphi}, \boldsymbol{\psi}, \tau) = \boldsymbol{\varphi}\big|_\tau - \boldsymbol{\psi}\big|_\tau = \int_0^\tau [\mathcal{L}(\boldsymbol{\varphi}) + \mathcal{E}(\boldsymbol{\varphi})]\,dt - \int_0^\tau \mathcal{L}(\boldsymbol{\psi})\,dt,$$

where $\mathcal{L}$ is a model operator and $\mathcal{E}$ is a model error operator. Thus $\mathcal{P}$ is a nonlinear operator about $\boldsymbol{\varphi}$ and $\boldsymbol{\psi}$, satisfying $\mathcal{P}: \mathbb{R}^n \times \mathbb{R}^n \rightarrow \mathbb{R}^n$.

The following discussion will prove the continuity of $\mathcal{P}(\boldsymbol{\varphi}, \boldsymbol{\psi}, \tau)$ on $\boldsymbol{\varphi}$ and $\boldsymbol{\psi}$, that is, $\forall \varepsilon > 0, \boldsymbol{\varphi}_0 \in \mathbb{R}^n, \boldsymbol{\psi}_0 \in \mathbb{R}^n, \exists \delta > 0$, whenever $\boldsymbol{\varphi} \in \mathbb{R}^n$, $\boldsymbol{\psi} \in \mathbb{R}^n$, $\|\boldsymbol{\varphi} - \boldsymbol{\varphi}_0\| < \delta$, $\|\boldsymbol{\psi} - \boldsymbol{\psi}_0\| < \delta$, such that $\|\mathcal{P}(\boldsymbol{\varphi}, \boldsymbol{\psi}, \tau) - \mathcal{P}(\boldsymbol{\varphi}_0, \boldsymbol{\psi}_0, \tau)\| < \varepsilon$.

To prove the theorem, two hypotheses are proposed.

Hypothesis 1: $\mathcal{L}(\boldsymbol{\varphi})$ and $\mathcal{E}(\boldsymbol{\varphi})$ are continuous about $\boldsymbol{\varphi}$; that is, $\forall \varepsilon > 0, \boldsymbol{\varphi}_0 \in \mathbb{R}^n, \exists \delta > 0$, whenever $\boldsymbol{\varphi} \in \mathbb{R}^n$, $\|\boldsymbol{\varphi} - \boldsymbol{\varphi}_0\| < \delta$, such that $\|\mathcal{L}(\boldsymbol{\varphi}) - \mathcal{L}(\boldsymbol{\varphi}_0)\| < \varepsilon$ and $\|\mathcal{E}(\boldsymbol{\varphi}) - \mathcal{E}(\boldsymbol{\varphi}_0)\| < \varepsilon$.

Hypothesis 2: $\boldsymbol{\varphi}(t)$ and $\boldsymbol{\psi}(t)$ are quasi periodical and uniform continuous about t; that is, $\forall \delta > 0$, $t_1, t_2 \in \mathbb{R}$, $k \in \mathbb{N}$, $\exists \alpha > 0$, whenever $kT < |t_1 - t_2| < kT + \alpha$, where T is the quasi period of $\boldsymbol{\varphi}(t)$ and $\boldsymbol{\psi}(t)$, such that $\|\boldsymbol{\varphi}(t_1) - \boldsymbol{\varphi}(t_2)\| < \delta$ and $\|\boldsymbol{\psi}(t_1) - \boldsymbol{\psi}(t_2)\| < \delta$.

Next, the rationality of these two hypotheses is discussed. First, in a numerical model, $\mathcal{L}$ is the time tendency of model variables and should be continuous to maintain the stability of a time-varying system; this means that the disturbance of model variables should not result in the drastic oscillation of tendency. Second, the sum of $\mathcal{L}$ and $\mathcal{E}$ can be viewed as the exact model tendency that is discretized from atmospheric equations and should satisfy the continuity strictly. From these two points, $\mathcal{E}$ is also continuous about $\boldsymbol{\varphi}$. Thus, hypothesis 1 is satisfied. With regard to hypothesis 2, the uniform continuity of $\boldsymbol{\varphi}(t)$ and $\boldsymbol{\psi}(t)$ about t is evident because real atmospheric evolution is a continuous process; the periodical hypothesis is rigorous in that atmosphere evolution is not exactly periodical. Fortunately, the historical analog state is known and the time T between the current initial state and analog state can be regarded as a quasi period. In this sense, the quasi-periodical hypothesis is reasonable. Because $\boldsymbol{\psi}(t)$ is integrated from the same initial field with $\boldsymbol{\varphi}(t)$, when the lead time τ is not too large, $\boldsymbol{\psi}(t)$ has approximate evolution and quasi period with $\boldsymbol{\varphi}(t)$. Then the proof of continuity theorem is as follows.

Proof

$\forall \varepsilon > 0, t_0, t_1 \in \mathbb{R}$ and $\exists \delta > 0, \alpha > 0, k \in \mathbb{N}$, whenever $kT < |t_0 - t_1| < kT + \alpha$, according to hypothesis 3 we can get $\|\boldsymbol{\varphi}_1 - \boldsymbol{\varphi}_0\| < \delta$ and $\|\boldsymbol{\psi}_1 - \boldsymbol{\psi}_0\| < \delta$. Based on hypotheses 1 and 2 and integral transformation, we can get

$$\begin{aligned}
\|\mathcal{P}(\boldsymbol{\varphi}_1, \boldsymbol{\psi}_1, \tau) - \mathcal{P}(\boldsymbol{\varphi}_0, \boldsymbol{\psi}_0, \tau)\| &= \left\| \int_{t_1}^{t_1+\tau} [\mathcal{L}(\boldsymbol{\varphi}) + \mathcal{E}(\boldsymbol{\varphi}) - \mathcal{L}(\boldsymbol{\psi})]\, dt - \int_{t_0}^{t_0+\tau} [\mathcal{L}(\boldsymbol{\varphi}) + \mathcal{E}(\boldsymbol{\varphi}) - \mathcal{L}(\boldsymbol{\psi})]\, dt \right\| \\
&= \left\| \int_0^{\tau} \{\mathcal{L}[\boldsymbol{\varphi}(t_1 + s)] + \mathcal{E}[\boldsymbol{\varphi}(t_1 + s)] - \mathcal{L}[\boldsymbol{\psi}(t_1 + s)]\}\, ds - \int_0^{\tau} \{\mathcal{L}[\boldsymbol{\varphi}(t_0 + s)] + \mathcal{E}[\boldsymbol{\varphi}(t_0 + s)] \right. \\
&\quad \left. - \mathcal{L}[\boldsymbol{\psi}(t_0 + s)]\}\, ds \right\| \le \int_0^{\tau} \|\mathcal{L}[\boldsymbol{\varphi}(t_1 + s)] - \mathcal{L}[\boldsymbol{\varphi}(t_0 + s)]\|\, ds + \int_0^{\tau} \|\mathcal{E}[\boldsymbol{\varphi}(t_1 + s)] \\
&\quad - \mathcal{E}[\boldsymbol{\varphi}(t_0 + s)]\|\, ds + \int_0^{\tau} \|\mathcal{L}[\boldsymbol{\psi}(t_0 + s)] - \mathcal{L}[\boldsymbol{\psi}(t_1 + s)]\|\, ds < 3\varepsilon\tau.
\end{aligned}$$

Let $\varepsilon^* \equiv 3\varepsilon\tau$. Because ε is random and τ is fixed, we can conclude that ε^* is randomly small. Therefore, the continuity is proven.

REFERENCES

Bao, M., Y. Ni, and J. Chou, 2004: The experiment of monthly mean circulation prediction using the analogue-dynamical model (in Chinese). *Chin. Sci. Bull.,* **49,** 1296–1300.

Barnett, T., and R. Preisendorfer, 1978: Multifield analog prediction of short-term climate fluctuations using a climate state vector. *J. Atmos. Sci.,* **35,** 1771–1787.

Chen, D. H., and Coauthors, 2008: New generation of multi-scale NWP system (GRAPES): General scientific design. *Chin. Sci. Bull.,* **53,** 3433–3445.

Chou, J., 1979: *Some Problems of Long-Term Numerical Weather Prediction* (in Chinese). Water Resources and Electric Power Press, 277 pp.

Dalcher, A., and E. Kalnay, 1987: Error growth and predictability in operational ECMWF forecasts. *Tellus,* **39A,** 474–491.

D'Andrea, F., and R. Vautard, 2000: Reducing systematic errors by empirically correcting model errors. *Tellus,* **52A,** 21–41.

Danforth, C. M., and E. Kalnay, 2008a: Impact of online empirical model correction on nonlinear error growth. *Geophys. Res. Lett.,* **35,** L24805, doi:10.1029/2008GL036239.

——, and ——, 2008b: Using singular value decomposition to parameterize state-dependent model errors. *J. Atmos. Sci.,* **65,** 1467–1478.

——, ——, and T. Miyoshi, 2007: Estimating and correcting global weather model error. *Mon. Wea. Rev.,* **135,** 281–299.

DelSole, T., and A. Y. Hou, 1999: Empirical correction of a dynamical model. Part I: Fundamental issues. *Mon. Wea. Rev.,* **127,** 2533–2545.

——, M. Zhao, P. A. Dirmeyer, and B. P. Kirtman, 2008: Empirical correction of a coupled land–atmosphere model. *Mon. Wea. Rev.,* **136,** 4063–4076.

Glahn, H. R., and D. A. Lowry, 1972: The use of model output statistics (MOS) in objective weather forecasting. *J. Appl. Meteor.,* **11,** 1203–1211.

Huang, J., and J. Chou, 1990: Studies on the analogous rhythm phenomenon in coupled ocean-atmosphere system. *Sci. China Chem.,* **33,** 851–860.

——, Y. Yi, S. Wang, and J. Chou, 1993: An analogue-dynamical long-range numerical weather prediction system incorporating historical evolution. *Quart. J. Roy. Meteor. Soc.,* **119,** 547–565.

Johansson, A., and S. Saha, 1989: Simulation of systematic error effects and their reduction in a simple model of the atmosphere. *Mon. Wea. Rev.,* **117,** 1658–1675.

Jung, T., 2005: Systematic errors of the atmospheric circulation in the ECMWF forecasting system. *Quart. J. Roy. Meteor. Soc.,* **131,** 1045–1073.

Kaas, E., A. Guldberg, W. May, and M. Déqué, 1999: Using tendency errors to tune the parameterisation of unresolved dynamical scale interactions in atmospheric general circulation models. *Tellus,* **51A,** 612–629.

Kalnay, E., 2002: *Atmospheric Modeling, Data Assimilation and Predictability.* Cambridge University Press, 364 pp.

Klinker, E., and P. D. Sardeshmukh, 1992: The diagnosis of mechanical dissipation in the atmosphere from large-scale balance requirements. *J. Atmos. Sci.,* **49,** 608–627.

Leith, C., 1978: Objective methods for weather prediction. *Annu. Rev. Fluid Mech.,* **10,** 107–128.

Li, K., 1986: Similarity difference degree and its technology (in Chinese). *Acta Meteor. Sin.,* **44,** 174–183.

Livezey, R. E., and A. G. Barnston, 1988: An operational multifield analog/antianalog prediction system for United States seasonal temperatures: 1. System design and winter experiments. *J. Geophys. Res.,* **93** (D9), 10 953–10 910.

Lorenz, E. N., 1969: Atmospheric predictability as revealed by naturally occurring analogues. *J. Atmos. Sci.,* **26,** 636–646.

Lynch, P., and X.-Y. Huang, 1992: Initialization of the HIRLAM model using a digital filter. *Mon. Wea. Rev.,* **120,** 1019–1034.

Qiu, C., and J. Chou, 1989: An analogue-dynamical method of weather forecasting (in Chinese). *Chin. J. Atmos. Sci.,* **13,** 22–28.

Ren, H., and J. Chou, 2007: Strategy and methodology of dynamical analogue prediction. *Sci. China Ser. D: Earth Sci.,* **50,** 1589–1599.

——, P. Zhang, W. Li, and J. Chou, 2006: A new method of dynamical analogue prediction based on multi-reference-state updating and its application. *Acta Phys. Sin.,* **55,** 4388–4396.

Reynolds, C. A., P. J. Webster, and E. Kalnay, 1994: Random error growth in NMC's global forecasts. *Mon. Wea. Rev.,* **122,** 1281–1305.

Saha, S., 1992: Response of the NMC MRF model to systematic-error correction within integration. *Mon. Wea. Rev.,* **120,** 345–360.

Van den Dool, H., 1994: Searching for analogues, how long must we wait? *Tellus,* **46A,** 314–324.

Yang, X.-Q., and J. L. Anderson, 2000: Correction of systematic errors in coupled GCM forecasts. *J. Climate,* **13,** 2072–2085.

Yang, X., T. DelSole, and H.-L. Pan, 2008: Empirical correction of the NCEP Global Forecast System. *Mon. Wea. Rev.,* **136,** 5224–5233.

Zhang, R. H., and X. S. Shen, 2008: On the development of the GRAPES—A new generation of the national operational NWP system in China. *Chin. Sci. Bull.,* **53,** 3429–3432.

Zheng, Z., J. Huang, G. Feng, and J. Chou, 2013: Forecast scheme and strategy for extended-range predictable components. *Sci. China Ser. D: Earth Sci.,* **56,** 878–889.